

1 **Genome-scale CRISPR Screens Identify Host Factors that Promote Human Coronavirus  
2 Infection**

3

4 **Authors:** Marco Grodzki<sup>1</sup>, Andrew P. Bluhm<sup>2,3</sup>, Moritz Schäfer<sup>4</sup>, Abderrahmane Tagmount<sup>5</sup>, Max  
5 Russo<sup>5,†</sup>, Amin Sobh<sup>6</sup>, Roya Rafiee<sup>7</sup>, Chris D. Vulpe<sup>5</sup>, Stephanie M. Karst<sup>1\*</sup>, Michael H. Norris<sup>2,3\*</sup>

6

7 **Affiliations:**

8 <sup>1</sup>Department of Molecular Genetics and Microbiology, College of Medicine, University of Florida;  
9 Gainesville, Florida, United States of America.

10 <sup>2</sup>Department of Geography, College of Liberal Arts and Sciences, University of Florida;  
11 Gainesville, Florida, United States of America.

12 <sup>3</sup>Emerging Pathogens Institute, University of Florida; Gainesville, Florida, United States of  
13 America.

14 <sup>4</sup>Institute for Molecular Health Sciences, Swiss Federal Institute of Technology in Zürich; Zurich,  
15 Switzerland.

16 <sup>5</sup>Department of Physiological Sciences, College of Veterinary Medicine, University of Florida;  
17 Gainesville, Florida, United States of America.

18 <sup>6</sup>University of Florida Health Cancer Center, University of Florida; Gainesville, Florida, United  
19 States of America.

20 <sup>7</sup>Department of Pharmacotherapy and Translational Research, College of Pharmacy, University of  
21 Florida; Gainesville, Florida, United States of America.

22 \*Corresponding author. Email: [skarst@ufl.edu](mailto:skarst@ufl.edu), [mhnorris@ufl.edu](mailto:mhnorris@ufl.edu).

23 †Present location: Department of Medical Oncology, Dana-Farber Cancer Institute, Harvard  
24 Medical School, Boston, Massachusetts, United States of America.

25 **One Sentence Summary:** Genome-wide CRISPR screens identified host factors that promote  
26 human coronavirus infection, revealing novel antiviral drug targets.

27

28 **Abstract:** The COVID-19 pandemic has resulted in 153 million infections and 3.2 million deaths  
29 as of May 2021. While effective vaccines are being administered globally, there is still a great  
30 need for antiviral therapies as potentially antigenically distinct SARS-CoV-2 variants continue to  
31 emerge across the globe. Viruses require host factors at every step in their life cycle, representing  
32 a rich pool of candidate targets for antiviral drug design. To identify host factors that promote  
33 SARS-CoV-2 infection with potential for broad-spectrum activity across the coronavirus family,  
34 we performed genome-scale CRISPR knockout screens in two cell lines (Vero E6 and HEK293T  
35 ectopically expressing ACE2) with SARS-CoV-2 and the common cold-causing human  
36 coronavirus OC43. While we identified multiple genes and functional pathways that have been  
37 previously reported to promote human coronavirus replication, we also identified a substantial  
38 number of novel genes and pathways. Of note, host factors involved in cell cycle regulation were  
39 enriched in our screens as were several key components of the programmed mRNA decay  
40 pathway. Finally, we identified novel candidate antiviral compounds targeting a number of factors  
41 revealed by our screens. Overall, our studies substantiate and expand the growing body of literature  
42 focused on understanding key human coronavirus-host cell interactions and exploit that knowledge  
43 for rational antiviral drug development.

44 **Main Text:**

45 **INTRODUCTION**

46 The COVID-19 pandemic is arguably the most consequential infectious disease outbreak in  
47 modern times. The causative agent of COVID-19, SARS-CoV-2, spread quickly across the planet  
48 resulting in 153 million infections and 3.2 million deaths at the time of this writing. Multiple  
49 COVID-19 vaccines recently demonstrated high efficacy, received FDA approval, and are being  
50 administered to people across the globe. While the importance of this scientific achievement  
51 cannot be understated, there is still a great need for novel antiviral therapies for use in vulnerable  
52 immunocompromised individuals, in regions where vaccine access is limited, and in the event that  
53 antigenically distinct SARS-CoV-2 variants emerge. Moreover, considering that SARS-CoV-2 is  
54 the third novel human coronavirus (HCoV) to emerge and cause serious disease in the human  
55 population in the past two decades following SARS-CoV and MERS-CoV, potent and broad-  
56 spectrum antivirals will leave us better prepared to deal with future pandemics. Broad-spectrum  
57 antivirals could also reduce morbidity associated with common cold-causing HCoVs including  
58 OC43, NL63, 229E, and HKU1.

59 Antivirals segregate into two basic categories, virus-targeting and host-targeting, both of which  
60 require an understanding of the molecular mechanisms used by viruses to replicate in host cells.  
61 Coronaviruses replicate via a well-established series of molecular events (1, 2). Host factors are  
62 required at every step in this life cycle and represent candidate druggable targets (i.e. host-targeting  
63 antivirals) with the potential for broad-spectrum activity against multiple viruses within a given  
64 virus family and even across virus families (3, 4). Accordingly, we performed CRISPR-based  
65 genome-wide knockout screens for both SARS-CoV-2 and OC43 infections to identify host factors  
66 that promote HCoV replication. Considering the power of genome-wide screens in the  
67 identification of host factors required for viral replication and the enormous global impact of the  
68 ongoing COVID-19 pandemic, it is not surprising that other research groups also applied this  
69 approach to SARS-CoV-2. Six genome-wide CRISPR screens for the identification of host factors  
70 promoting SARS-CoV-2 replication are published (5–10). Despite the redundancy in overall  
71 approach, there was experimental variability across screens in the selection of cell lines and  
72 infection conditions. Together with the sheer magnitude of critical host-virus interactions required  
73 for successful viral infection, individual screens are likely to capture only a subset of these host  
74 factors. Consistent with this, while specific genes and pathways were identified across published  
75 studies, each study also provided unique findings which expand our understanding of host-HCoV  
76 interactions.

77 In this study, we report a global analysis of host-HCoV interactions gleaned from genome-  
78 wide screens performed for two HCoVs and in two different cell lines. We also performed a  
79 comprehensive comparative analysis of all published genome-wide SARS-CoV-2 screens to date.  
80 Multiple genes and functional pathways identified in our screens were previously reported to  
81 promote SARS-CoV-2 replication, validating the rigor of our approach and providing further  
82 support for the role of specific host factors. Yet we also identified a substantial number of novel  
83 genes and pathways not previously reported to promote HCoV replication. We validated the  
84 importance of a subset of genes identified in these screens in HCoV replication. Notably, several  
85 of the novel host factors identified in our study provide unique insight into SARS-CoV-2  
86 replication processes that could be targeted with antiviral drugs. Host factors involved in cell cycle  
87 regulation were enriched in our screens and we show that compounds (abemaciclib, AZ1 protease  
88 inhibitor, harmine, nintedanib, and UC2288) targeting these host factors inhibit *in vitro* HCoV

89 replication. We also identified multiple host factors involved in endocytosis and TBK1 that plays  
90 a key role in innate immune responses. Inhibitors of these processes/factors (promethazine and  
91 amlexanox, respectively) also displayed antiviral activity. Together, our study has provided  
92 significant insight into host-HCoV interactions and identified novel candidate antiviral  
93 compounds.

94

## 95 RESULTS

96

### 97 **Genome-wide CRISPR screens in Vero E6 cells identify host factors required for HCoV 98 infection**

99 In order to identify host factors that promote HCoV infection, we performed genome-wide  
100 loss of function CRISPR screens for pathogenic SARS-CoV-2 and common cold-causing OC43  
101 in two susceptible cell lines. Due to the highly cytopathic nature of HCoV infection in the Vero  
102 E6 cells derived from African Green Monkey (AGM; *Chlorocebus sabaeus*), we carried out  
103 genome-wide screens using a custom Vervet CRISPR knockout library (see supplemental  
104 methods) (**Fig. 1A**). Vero E6 cells were transduced with the Vervet CRISPR library and infected  
105 with SARS-CoV-2 or OC43 at a multiplicity of infection (MOI) 0.01. We observed ~60% visible  
106 cytopathic effect (CPE) for SARS-CoV-2 and ~85% CPE for OC43. Resistant clones were  
107 expanded, reinfected with the corresponding virus at MOI 0.1, and re-expanded. Genomic DNA  
108 was extracted from surviving cells, sgRNAs amplified, and sequenced. We carried out MAGeCK  
109 analysis to identify genes targeted by significantly enriched sgRNAs which are labeled in the  
110 volcano plots in **Figs. 2A-B**. To facilitate the access and reusability of data sets generated from  
111 genome-scale CRISPR screens in HCoV-infected cells, we have also hosted a website  
112 ([sarscrisprscreens.epi.ufl.edu](http://sarscrisprscreens.epi.ufl.edu)) with the complete set of MAGeCK results for each of the screens  
113 described in this study and data from previously published screens reanalyzed herein (3, 7–10).  
114 The website was designed to facilitate integration of upcoming screens and we hope for  
115 contributions to drive this as a community project.

116 We identified multiple candidate host factors previously demonstrated to play a functional  
117 role in SARS-CoV-2 and OC43 infections. For example, *ACE2* was identified in the SARS-CoV-  
118 2 screen (11). Furthermore, *TMEM41B* was a top-scoring gene in the OC43 screen, supporting  
119 recent work by Schneider et al. demonstrating that *TMEM41B* is a pan-HCoV host factor (7). We  
120 also identified interferon (IFN)-induced transmembrane (IFITM) proteins that have been reported  
121 to regulate HCoV infection (12–14). Genes targeted by significantly enriched sgRNAs (FDR<0.1)  
122 were next segregated into functional categories listed in tables in **Figs. 2C-2D**. Of note, *CDK4*, a  
123 master regulator of cell cycle, was identified as a key host factor for both viruses. Disruption of  
124 additional genes encoding regulators of cell cycle progression, including *CDK1A*, *DYRK1A*,  
125 *HRK* and *P53*, similarly increased cellular resistance to SARS-CoV-2 infection.

126 During the completion of our studies, Wei et al. reported similar SARS-CoV-2 screens in  
127 Vero E6 cells performed with an independent sgRNA library based on an earlier *C. sabaeus*  
128 genome assembly (8). In order to compare our data sets to those of Wei et al., we downloaded raw  
129 data from their study and analyzed them using MAGeCK-VISPR (8, 15). There were 6 targeted  
130 genes identified in common between studies: *ACE2*, *DPF2*, *DYRK1A*, *RAD54L2*, *SMARCA4*, and  
131 *TP53*.

132

133 **Genome-wide CRISPR screens in HEK293T-hACE2 cells identify host factors required for**  
134 **HCoV infection**

135 We similarly performed CRISPR screens in human HEK293T cells ectopically expressing  
136 the human ACE2 receptor (HEK293T-hACE2) transduced with the Brunello sgRNA library (16)  
137 (**Fig. 1B**). Transduced cells were infected with SARS-CoV-2 or OC43 at MOI 0.01. SARS-CoV-  
138 2-infected cultures developed ~40% CPE and OC43-infected cultures developed >85% CPE.  
139 Resistant cell populations propagated to confluence were reinfected with the corresponding virus  
140 at either MOI 0.01 or MOI 0.1 and re-expanded. Genomic DNA was extracted and sgRNAs from  
141 both the initial and secondary infections were sequenced.

142 The genes targeted by the most highly enriched sgRNAs in each of the SARS-CoV-2  
143 infections are indicated in **Figs. 3A-3C**. *EDC4*, a gene encoding a scaffold protein that functions  
144 in programmed mRNA decay, was the overall top-scoring gene. Interestingly, *XRN1* encodes  
145 another key player in this pathway and was also top-scoring. We further categorized the genes  
146 encoding candidate host factors (FDR<0.1) into functional categories depicted in heat maps in **Fig.**  
147 **3D**. Consistent with other published screens, we identified multiple components of the endocytic  
148 pathway including *CCZ1*, *DNM2*, and *WASL*. Other functional categories in which multiple genes  
149 were identified include cell adhesion, cell cycle, integrator complex, lysosome, mTOR regulation,  
150 and ubiquitination/proteolysis. We carried out an independent SARS-CoV-2 screen using the  
151 higher MOI of 0.3 for initial infection which resulted in ~80% CPE, and MOI 0.03 for secondary  
152 infection. Genes targeted by the most significantly enriched sgRNAs in this study are presented in  
153 **Figs. 3E-3F** and are segregated into functional categories depicted in heat maps in **Fig. 3G**. *ACE2*  
154 was a top-scoring gene in this screen. Functional categories with multiple targeted genes include  
155 amphisome, autophagy, endosome, exocytosis, lysosome, peroxisome,  
156 transcription/transcriptional regulation, and ion transporters. *C18orf8*, *CCZ1*, *CDH2*, and  
157 *TMEM251* were identified in both the low- and high-MOI SARS-CoV-2 screens.

158 The genes targeted by the most highly enriched sgRNAs in the OC43 HEK293T-hACE2  
159 screens are indicated in **Figs. 4A-4C** and segregated into functional categories in **Fig. 4D**. As  
160 expected, based on prior work, genes encoding IFITM proteins were identified as proviral factors  
161 for OC43 (12). *TMEM41B* was a top-scoring gene along with the functionally related *VMP1*, as  
162 were *CCZ1*, *CCZ1B*, *SLC35B2*, and *WDR81* which have all been reported in other recent OC43  
163 genome-wide screens (6, 7). When comparing the SARS-CoV-2 and OC43 HEK293T-hACE2  
164 datasets, there were 6 genes in common targeted by significantly enriched sgRNAs (*C18orf8*,  
165 *CCZ1*, *CCZ1B*, *RAB7A*, *WDR81*, and *WDR91*). Notably, all of the corresponding gene products  
166 function in vesicle-mediated transport.

167 During the completion of our studies, similar SARS-CoV-2 screens in human Huh-7.5 (6,  
168 7, 10) and A549 (5, 9) cells were published. In order to compare our data sets to those of other  
169 groups, we downloaded raw data from four published studies (6, 7, 9, 10), analyzed them using a  
170 common analysis framework (MAGECK) and stringency (FDR<0.25) and compared the results to  
171 our data sets. Using this stringency, no genes were identified in all five studies, 1 gene was  
172 identified in four studies (*ACE2*), 6 genes were identified in three studies (*VPS35*, *CTSL*, *DNM2*,  
173 *CCZ1B*, *TMEM106B*, and *VAC14*), and 25 genes were identified in two studies (*ALG5*, *ARVCF*,  
174 *ATP6V1A*, *ATP6V1G1*, *B3GAT3*, *CNOT4*, *EPT1*, *EXOC2*, *EXT1*, *EXTL3*, *GDI2*, *LUC7L2*,  
175 *MBTPS2*, *PIK3C3*, *RAB7A*, *RNHI*, *SCAF4*, *SCAP*, *SLC30A1*, *SLC33A1*, *SNX27*, *TMEM41B*,  
176 *TMEM251*, *WDR81*, and *WDR91*) (**Fig. 5A-5B**). It should be noted that these genes were top-  
177 scoring across studies performed in different human cell lines, suggesting they are broadly  
178 important in SARS-CoV-2 replication. Shared pathways include vesicle-mediated transport

179 (*CCZ1B*, *DNM2*, *EXOC2*, *GDI2*, *PIK3C3*, *RAB7A*, *SNX27*, *VAC14*, *VPS35*, *WDR81*, *WDR91*),  
180 vacuolar ATPases important in organelle acidification (*ATP6VIA*, *ATP6V1E*, *ATP6V1G1*), and  
181 heparan sulfate biosynthesis genes (*EXT1*, *EXTL3*, *B3GAT3*). We identified 53 genes targeted by  
182 enriched sgRNAs in our study that were not identified in published studies (**Fig. 5C**), including  
183 *EDC4* and *XRN1*.

184  
185 **Validation of a subset of gene candidates that promote human coronavirus replication**  
186 To confirm that unique genes identified in our screens promote HCoV replication,  
187 HEK293T-hACE2 cells were engineered to stably express gene-specific shRNAs targeting *CCZ1*  
188 or *EDC4*. *CTSL* knockdown was tested as a positive control for SARS-CoV-2 (17). Efficiency of  
189 gene knockdown assessed by western blotting was robust for all three genes (**Fig. 6A**). Knockdown  
190 cells were then infected with SARS-CoV-2 or OC43 and viral genome copy number determined  
191 at 2 days post-infection (dpi). All three genes were required for optimal SARS-CoV-2 infection  
192 while *CCZ1* and *EDC4*, but not *CTSL*, promoted OC43 infection (**Fig. 6B**).  
193

#### 194 **CRISPR screening reveals novel antiviral drugs displaying *in vitro* efficacy**

195 We next determined whether gene products and pathways identified in our screens could  
196 be targeted with commercially available inhibitors to block HCoV infection. Numerous genes  
197 involved in cell cycle regulation were identified in our screens. The following inhibitors targeting  
198 this class of host factors were tested: abemaciclib (ABE; Cdk4 inhibitor), UC2288 (UC2;  
199 CDKN1A/p21 inhibitor), harmine (HAR) and INDY (Dyrk1A inhibitors), AZ1 (Usp25/28  
200 inhibitor), olaparib (OPB; ARID1A inhibitor), and nintedanib (NIN; FGFR1/2/3 inhibitor). Host  
201 factors involved in endocytosis have been widely reported to regulate HCoV replication and were  
202 identified in our and others' CRISPR screens (18) so we also tested several drugs targeting this  
203 process including CID1067700 (CID; Rab7a inhibitor), chlorpromazine (CPZ; Wdr81 inhibitor),  
204 and promethazine (PMZ; Wdr81 inhibitor). Finally, we tested amlexanox (AMX) which inhibits  
205 TANK binding kinase 1 (TBK1) and its adaptor protein TBK-binding protein 1 (TBKBP1) which  
206 has been reported to variously regulate Rab7a activity (19) or induction of IFN response genes  
207 (20). The heat map in **Fig. 7A** shows the fold-enrichment of sgRNAs targeting the genes of interest  
208 across the screens performed in this study.

209 In an initial experiment of the entire panel of small molecules, inhibitors were added to  
210 culture supernatants at the initiation of SARS-CoV-2 infection and evaluated for their capacity to  
211 inhibit virus-induced CPE at 3 dpi in Vero E6 cells. The concentrations of inhibitors used, based  
212 on available toxicity data, were generally nontoxic in Vero E6 cells (**Fig. 7B, white bars**). ABE,  
213 AMX, HAR, NIN, OPB, PMZ, and UC2 significantly inhibited virus-induced cytotoxicity while  
214 AZ1, CPZ, INDY, and CID did not (**Fig. 7B, gray bars**). Our CID results are consistent with prior  
215 work which showed reduced CoV egress, but no effect on cell viability or viral replication, in  
216 response to CID treatment (2). Although INDY and HAR both target Dyrk1A, only HAR displayed  
217 activity in this assay, potentially due to the lower enzymatic IC<sub>50</sub> of HAR for Dyrk1A (0.24 μM  
218 for INDY vs. 0.08 μM for HAR). As a complementary approach to measure antiviral activity of  
219 these compounds, we quantified viral genome copies by RT-qPCR in cells treated with each  
220 compound at 2 dpi. ABE, AMX, HAR, PMZ and UC2 significantly decreased viral genome copy  
221 number (**Fig. 7C**), consistent with their ability to protect from virus-induced cytotoxicity. On the  
222 other hand, NIN and OPB had no effect on viral genome copy number despite their moderate  
223 inhibition of SARS-CoV-2-induced cytotoxicity. Conversely, AZ1 completely inhibited viral  
224 genome replication in spite of having no significant effect on cytotoxicity.

225 For compounds displaying activity in one or both of these assays, we next determined their  
226 EC<sub>50</sub> and IC<sub>50</sub> against SARS-CoV-2 infection by cytotoxicity measurements in the presence or  
227 absence of virus across a series of inhibitor dilutions (**Figs. 7D-J**). Several of the inhibitors had  
228 EC<sub>50</sub> values below 20  $\mu$ M (10.86  $\mu$ M for ABE, 14.1  $\mu$ M for NIN, and 2.16  $\mu$ M for UC2), with the  
229 p21 inhibitor UC2 being the most potent. AMX is typically used as topical treatment and had a  
230 high EC<sub>50</sub> at 342.96  $\mu$ M. AZ1 (37.49  $\mu$ M), HAR (61.44  $\mu$ M) and PMZ (88.41  $\mu$ M) showed  
231 intermediate EC<sub>50</sub> levels. Overall, these findings reveal novel candidates for anti-HCoV drug  
232 development.

233

## 234 **DISCUSSION**

235 Genome-wide CRISPR knockout screens have been very successful in identifying host  
236 factors required for viral infection so it is not surprising that this approach has been applied to the  
237 discovery of proviral factors for SARS-CoV-2 infection. Indeed, six recent studies have reported  
238 CRISPR screens in cells infected with SARS-CoV-2 (5–10). As has been observed generally for  
239 genome-wide screens, there was limited overlap in the set of genes reported as host factors. In our  
240 reanalysis of the data using a common framework, there were only 17 genes identified in two or  
241 more published screens performed in human cells (*ACE2*, *ATP6V1A*, *ATP6V1G1*, *B3GAT3*,  
242 *CCZ1B*, *CNOT4*, *CTSL*, *DNM2*, *EXOC2*, *EXT1*, *EXTL3*, *MBTPS2*, *PIK3C3*, *SCAP*, *TMEM106B*,  
243 *VAC14*, and *VPS35*). This finding is not unexpected considering that the screens were performed  
244 in a variety of cell lines and under varying infection conditions. There was more overlap in the  
245 functional categories identified across studies, with enrichment of genes involved in  
246 glycosaminoglycan biosynthesis, vesicle transport, and ER/Golgi-localized proteins (18). Due to  
247 the limited redundancy of specific host factors identified across published studies and the potential  
248 of proviral gene products to be targeted with antiviral drugs, additional genome-wide screens are  
249 warranted. To that end, we performed CRISPR screens in AGM Vero E6 cells and human  
250 HEK293T-hACE2 cells. We performed screens for both SARS-CoV-2 and the common cold-  
251 causing HCoV OC43 to increase the probability of identifying pan-HCoV proviral factors  
252 representing strong targets for developing broad-spectrum antivirals. Our study provides  
253 additional support for previously identified candidate host factors and reports multiple novel host  
254 factors and pathways playing potentially key roles in viral replication. We summarize the  
255 consolidated set of candidate host factors identified for SARS-CoV-2 in our study as well as those  
256 identified in two or more studies in **Fig. 8**.

257 Host factors promoting SARS-CoV-2 infection of Vero E6 cells (FDR<0.25) are indicated  
258 in **Fig. 8** adjacent to the presumptive step in the viral life cycle in which they function. In this cell  
259 line, cell cycle regulation was key to SARS-CoV-2 replication. *CDK4* was a top-scoring gene for  
260 both SARS-CoV-2 and OC43, suggesting it is broadly required for HCoV replication. CoVs utilize  
261 diverse strategies to manipulate the host cell cycle to promote their replication (21). Identification  
262 of specific cell cycle-related host factors required for HCoV replication could provide clues to  
263 dissecting viral regulatory mechanisms. We also identified IFITM proteins in both SARS-CoV-2  
264 and OC43 screens in Vero E6 cells, consistent with a prior study reporting that IFITM proteins  
265 promote OC43 infection (12). Interestingly, recent work suggests that IFITM proteins promote  
266 HCoV entry when it occurs at the plasma membrane but inhibit HCoV entry when it occurs in the  
267 endocytic pathway (13, 14), suggesting that HCoVs enter Vero E6 cells primarily at the plasma  
268 membrane instead of using the endosomal pathway. This finding is consistent with the paucity of  
269 factors involved in endocytosis identified in these screens, in stark contrast to our and others'  
270 results in screens performed in human cell lines.

271 In addition to CDK4 and IFITM proteins, targeting of *SLC35B2* in both SARS-CoV-2 and  
272 OC43 Vero E6 screens increased resistance to infection, suggesting that it is a pan-HCoV host  
273 factor in this cell line. *SLC35B2* encodes 3'-phosphoadenosine 5'-phosphosulfate transporter 1  
274 (PAPST1) which plays an important role in heparan sulfate biosynthesis. PAPST1 is required for  
275 optimal replication of a variety of viruses including HIV, dengue virus, and bunyaviruses, enabling  
276 heparan sulfate-mediated viral entry or sulfating a viral receptor that enables virion binding (22–  
277 24). It is hence logical to predict that it functions in HCoV entry in Vero E6 cells as well.  
278 Additional candidate pan-HCoV factors identified in the Vero E6 studies include *PLN* encoding  
279 phospholamban and *C16orf74* which are both implicated in maintaining calcium homeostasis (25–  
280 27), and *C3orf80* encoding a protein of unknown function. None of these gene products have been  
281 previously identified as viral host factors to our knowledge, and their functional roles will require  
282 further study.

283 Host factors promoting SARS-CoV-2 infection of HEK293T-hACE2 cells (FDR<0.25) are  
284 indicated in **Fig. 8** adjacent to the presumptive step in the viral life cycle in which they function.  
285 The functional categories with the most top-scoring genes were vesicle transport, cell cycle  
286 regulation, autophagy, and ubiquitination/proteolysis. For the OC43 screens, the most abundant  
287 functional categories were vesicle transport, transcriptional regulation including the SWI/SNF  
288 complex, innate immunity, and transporters. The host factors identified in the HEK293T-hACE2  
289 screens for both SARS-CoV-2 and OC43 (*C18orf8*, *CCZ1*, *CCZ1B*, *RAB7A*, *WDR81*, and  
290 *WDR91*) are all involved in vesicle-mediated transport and particularly in endosomal maturation,  
291 underscoring the importance of this process for HCoV infection.

292 When comparing our SARS-CoV-2 data sets in HEK293T-hACE2 cells to published data  
293 sets in other human cell lines, there were 21 genes in common with other studies (FDR<0.25;  
294 *ACE2*, *ALG5*, *ARVCF*, *CCZ1B*, *CTSL*, *DNM2*, *EPT1*, *GDI2*, *LUC7L2*, *RAB7A*, *RNH1*, *SCAF4*,  
295 *SLC30A1*, *SLC33A1*, *SNX27*, *TMEM41B*, *TMEM251*, *VAC14*, *VPS35*, *WDR81*, and *WDR91*)  
296 which highlight key functional pathways required for viral infection, including endocytosis,  
297 glycosylation, and exocytosis. Remarkably though, we identified 53 unique genes, underscoring  
298 the importance of continued screening to fully elucidate host factors promoting SARS-CoV-2  
299 replication. Certain unique genes function in previously identified pathways such as vesicle  
300 transport (e.g., *CCZ1*, *C18orf8*) and ER/Golgi-localized proteins (e.g., *SEC63*, *ERGIC3*). Other  
301 unique genes function in processes that have not been previously described as proviral in HCoV  
302 infections. For example, *EDC4* was a top-scoring gene in our SARS-CoV-2 screens in HEK293T-  
303 hACE2 cells. *EDC4* functions as a scaffold protein for the assembly of the programmed mRNA  
304 decay complex. Although it has not been reported to play a role in HCoV infection before, it does  
305 promote rotavirus replication complex assembly (28). Another component of the programmed  
306 mRNA decay pathway *XRN1* was also modestly enriched, suggesting that this pathway promotes  
307 SARS-CoV-2 replication. Alternatively, *EDC4* and *XRN1* are both P-body components. Many  
308 RNA viruses interact with and hijack P-bodies in order to promote viral replication (29) and SARS-  
309 CoV-2 has recently been reported to disrupt P-bodies (30) so it is possible that the virus interacts  
310 with these host factors to disassemble P-bodies and facilitate viral replication. We also identified  
311 three unique genes encoding factors involved in targeting proteins to lysosomes – *GNPTAB*,  
312 *GNPTG*, and *NAGPA*. Considering recent progress in understanding the key role played by  
313 lysosomes in HCoV egress (2), it is interesting to speculate that HCoVs interact with these proteins  
314 to facilitate virion release from the infected cell.

315 Two approaches were taken to validate the proviral role of a subset of unique host factors  
316 identified in our screens. First, shRNA-mediated knockdown of *CCZ1* and *EDC4* resulted in

317 reduced SARS-CoV-2 and OC43 replication. Second, drugs targeting selected host factors  
318 displayed antiviral efficacy *in vitro* against SARS-CoV-2. These include cell cycle inhibitors ABE  
319 targeting Cdk4, AZ1 targeting Usp25/28, HAR targeting Dyrk1A, NIN targeting Fgfr1/2/3, and  
320 UC2 targeting p21; the endocytosis inhibitor PMZ targeting Wdr81; and the Tbk1 inhibitor AMX.  
321 Chen et al. recently reported similar activity of ABE against SARS-CoV-2 (31), validating our  
322 findings. To our knowledge, the discovery that AMX, AZ1, HAR, NIN, PMZ, and UC2 possess  
323 antiviral activity against SARS-CoV-2 has not been reported. AMX, PMZ, and NIN are currently  
324 available drugs which could potentially be repurposed, while HAR is a natural product being  
325 investigated for the treatment of a variety of diseases. While no clinical therapeutics are currently  
326 available targeting p21 or Usp25/28, our data suggest that these could be worthwhile targets for  
327 drug development. Further study of the potential *in vivo* utility of these compounds in treating  
328 HCoV infections and their mechanism of action is warranted.

329 Our studies substantiate and expand the growing body of literature focused on  
330 understanding key HCoV-host cell interactions. The fairly limited redundancy in proviral factors  
331 identified across our study and other published studies using genome-wide CRISPR screens (5–  
332 10) highlights the extensive scope of these interactions and suggests that even more host factors  
333 remain to be discovered. Cell type differences and variable infection conditions undoubtedly  
334 influence the outcomes of screens and could provide novel insight into nuanced viral replication  
335 mechanisms. For example, we identified lysosomal proteins as proviral in HEK293T-hACE2 cells  
336 but not in Vero E6 cells, raising the possibility that there are cell type-specific differences in the  
337 use of lysosomes for HCoV egress (2). Detailed molecular studies testing hypotheses like this  
338 stemming from genome-scale CRISPR screens are a critical next step. Similarly, although we have  
339 identified novel compounds displaying antiviral activity against HCoVs *in vitro*, additional work  
340 is needed to determine their mechanism of action at the molecular level and *in vivo* efficacy before  
341 they can be applied in the clinic.

342

## 343 MATERIALS AND METHODS

344

### 345 Study design

346 The objectives of this study were to identify host factors that promote HCoV replication and to  
347 determine whether these host factors can be targeted with commercially available drugs to block  
348 viral infection *in vitro* (Fig. S1). To achieve this goal, we performed genome-wide CRISPR  
349 knockout screens in Vero E6 cells using a newly generated Vervet sgRNA library (Fig. 1A) and  
350 in HEK293T-hACE2 cells using the commercially available human Brunello sgRNA library (Fig.  
351 1B). In brief, cells transduced with sgRNA libraries were infected with HCoVs, SARS-CoV-2 and  
352 OC43, using various MOIs. Cells surviving infection were expanded and re-infected, and the  
353 sgRNAs enriched in resistant clones was determined. Genes targeted by enriched sgRNAs were  
354 compared between replicates, infection conditions, HCoVs, cell lines, and previously published  
355 screens to identify common and unique host factors as well as putative pan-HCoV host factors.  
356 Genes of interest were selected for validation and targeted for knockdown using shRNAs followed  
357 by infection with HCoVs. Commercially available inhibitors to other important genes identified in  
358 our study were evaluated for their capacity to prevent virus-induced toxicity and viral replication  
359 *in vitro*. EC<sub>50</sub> and IC<sub>50</sub> values for efficacious compounds were determined.

360

361

362 **Virus stock generation and titer determination**

363 SARS-CoV-2 strain UF-1 (GenBank accession number MT295464.1) was originally isolated from  
364 a COVID-19 patient at the University of Florida Health Shands Hospital via nasal swab (32) and  
365 manipulated in a Biosafety Level 3 (BSL3) laboratory at the Emerging Pathogens Institute under  
366 a protocol approved by the University of Florida Institutional Biosafety Committee. The HCoV  
367 OC43 strain was a kind gift from Dr. John Lednicky (University of Florida). SARS-CoV-2 and  
368 OC43 were propagated in Vero E6 cells (ATCC) grown in Dulbecco's Modified Eagle Medium  
369 (DMEM; Gibco) supplemented with 10% heat inactivated fetal bovine serum (FBS; Atlanta  
370 Biologicals) and Pen-Strep (100 U/ml penicillin, 100 µg/ml streptomycin; Gibco) at 37°C and 5%  
371 CO<sub>2</sub>. Virus stocks were prepared by infecting Vero E6 cells at MOI 0.01, centrifuging culture  
372 supernatants collected at 3 dpi for 5 mins at 1000 x g, and filtering through a 0.44 µm PVDF filter  
373 (Millipore) followed by a 0.22 µm PVDF filter (Restek). The virus stocks were aliquoted and  
374 stored at -80°C. Virus stocks were titered using a standard TCID<sub>50</sub> assay. In brief, Vero E6 cells  
375 were seeded at 2x10<sup>4</sup> cells per well in a 96-well plate (Corning) and allowed to attach overnight.  
376 Virus stocks were serially diluted onto cells, with a total of 8 replicates per dilution. Monolayers  
377 were visualized in the BSL3 using an EVOS XL Core microscope (Thermo Fisher Scientific) and  
378 scored positive or negative for cytopathic effect (CPE) at 7 dpi.  
379

380 **Viral genome copy number enumeration**

381 For SARS-CoV-2, supernatants and cells were harvested into AVL buffer from the QIAamp Viral  
382 RNA Kit (Qiagen) and RNA was purified according to the manufacturer's recommendations. The  
383 samples underwent reverse transcription and cDNA synthesis using the iTaq Universal SYBR  
384 Green One-Step Kit (BioRad) and primers targeting the nucleocapsid (N) gene of SARS-CoV-2  
385 (NproteinF- GCCTCTTCTCGTTCATCAC, NproteinR-AGCAGCATCACCGCCATTG).  
386 qPCR was carried out on a Bio-Rad CFX96 and viral genome copy numbers were extrapolated  
387 using CT values from a standard curve generated using a control plasmid containing the N protein  
388 gene (Integrated DNA Technologies). For OC43, RNA from infected cells was purified using the  
389 RNeasy Mini Kit (Qiagen) according to the manufacturer's recommendations and amplified using  
390 the Applied Biosystems AgPath-ID One-Step RT-PCR Kit (Thermo Fisher Scientific) and primers  
391 and probe targeting the N gene of OC43 (33). GAPDH levels were determined for each sample for  
392 normalization purposes using previously described primers (34). All samples were run in triplicate  
393 for each primer pair and normalized viral genome copy numbers were calculated using the  
394 comparative cycle threshold method.  
395

396 **Genome-wide CRISPR sgRNA screens**

397 The human CRISPR Brunello library (Addgene 73178) (16) was amplified following a previously  
398 published protocol (35). We constructed a Vervet domain-targeted sgRNA library since one was  
399 not commercially available. Detailed methods are reported in supplemental material. For both  
400 libraries, lentiviruses were produced in HEK293T cells by co-transfection of library plasmids  
401 together with the packaging plasmid psPAX2 (Addgene 12260) and envelope plasmid pMD2.G  
402 (Addgene 12259). CRISPR screens were carried out in two cell lines (outlined in **Fig. 1**): AGM  
403 Vero E6 cells were transduced with the newly generated Vervet sgRNA library and human  
404 HEK293T-hACE2 cells (Genecopoeia) were transduced with the Brunello sgRNA library. For  
405 each screen, 1.2x10<sup>8</sup> cells were transduced with lentivirus-packaged sgRNA library at MOI 0.3 in  
406 the presence of 8 µg/ml polybrene (Sigma) to achieve ~500-fold overrepresentation of each  
407 sgRNA. After 48 h, 0.6 µg/ml puromycin (Gibco) was added to eliminate non-transduced cells

408 and cultures were expanded in Matrigel-coated (Corning) T300 flasks. Control replicates were  
409 collected at this time to determine input library composition and additional replicates were infected  
410 with SARS-CoV-2 or OC43 at the indicated MOIs. Cells surviving initial infections were collected  
411 when they had expanded to confluence. A portion of each replicate was stored in DNA/RNA  
412 Shield (Zymo Research) at -80°C for genomic DNA extraction and the remaining cells were  
413 reseeded and reinfected at the indicated MOIs. Cells surviving reinfections were also harvested at  
414 confluence for genomic DNA extraction.

415  
416 Genomic DNA was extracted from each sample (detailed extraction methods are described in  
417 supplemental methods). The sgRNA regions were then amplified and indexed for Illumina  
418 sequencing using a one-step PCR method and primers specific to the LentiCRISPRv2-based  
419 Vervet and Brunello libraries. Primers and indices used for the generation of amplicon libraries  
420 are listed in **Table S1**. Brunello and Vervet DNA samples were amplified in ten 100 µl reactions  
421 using the NEBNext High-Fidelity 2X Master Mix Kit (New England Biolabs), 0.5 µM of forward  
422 and reverse primers and 10 µg of DNA template per reaction with the following program: initial  
423 denaturation at 98°C for 3 min, 24 cycles of denaturation at 98°C for 10 s, annealing 60°C for 15  
424 s and extension 72°C for 25 s, and final extension at 72°C for 2 min. 256 bp amplicons were  
425 quantified on a 2% agarose gel stained with SYBR Safe (Invitrogen), using the Gel Doc  
426 quantification software (Bio-Rad). Amplicons were first pooled in an equimolar fashion and then  
427 the pools were gel-extracted using the PureLink Quick Gel Extraction Kit (Thermo Fisher  
428 Scientific). The sequencing was carried out at the Interdisciplinary Center for Biotechnology  
429 Research (ICBR; University of Florida) using a NovaSeq 6000 sequencer (Illumina). The Brunello  
430 amplicons were sequenced using the S4 2X150 cycles Kit (Illumina) while the Vervet-AGM  
431 amplicons were sequenced with the SP 1X100 cycles Kit (Illumina).

432  
433 **Computational analysis**  
434 The FASTX-Toolkit was used to demultiplex raw FASTQ data which were further processed to  
435 generate reads containing only the unique 20 bp sgRNA sequences. The sgRNA sequences from  
436 the library were assembled into a Burrows-Wheeler index using the Bowtie build-index function  
437 and reads were aligned to the index. The efficiency of alignment was checked and the number of  
438 uniquely aligned reads for each library sequence was calculated to create a table of raw counts.  
439 Ranking of genes corresponding to perturbations that are enriched in infected cultures was  
440 performed using a robust ranking aggregation (a-RRA) algorithm implemented in the Model-based  
441 Analysis of Genome-wide CRISPR/Cas9 Knockout (MAGECK) tool through the test module.  
442 Tables with raw counts corresponding to each sgRNA in reference (initial pool) and selected  
443 (virus-infected) samples were used as an input for MAGECK test. Gene-level ranking was based  
444 on FDRs and candidates with FDRs < 0.25 were considered as significant hits. Ranking of genes  
445 corresponding to positively selected and negatively selected perturbations was performed using a  
446 robust ranking aggregation (a-RRA) algorithm implemented in MAGECK through the test module  
447 (36). Tables with raw counts corresponding to each sgRNA in reference (initial pool) and selected  
448 (exposed to virus) samples were used as an input for MAGECK test. Gene-level ranking was based  
449 on false discovery rate (FDR) and candidates with FDR < 0.25 were considered as significant hits.  
450 Additional details can be found in the supplementary methods. We submitted FastQ files to Gene  
451 expression omnibus (GSE: XXXXXX) and all CRISPR screen data to BioGRID ORCS database  
452 (<https://orcs.thebiogrid.org/>). In addition, all data is available at [sarscrisprscreens.epi.ufl.edu](https://sarscrisprscreens.epi.ufl.edu).

453  
454

455 **Validation of host factors in promoting viral infections**

456 To validate selected host factors for their capacity to promote HCoV infection *in vitro*, we  
457 transduced HEK293T-hACE2 cells with lentivirus-packaged shRNAs targeting *CTSL*, *CCZ1*, or  
458 *EDC4* (TRC Human shRNA Library collection) or the empty vector pLKO.1. Transduced cells  
459 were expanded under puromycin selection (0.8 ug/ml) for at least 7 days to generate stable  
460 knockdown cell lines. To confirm knockdown, cell lysates prepared from knockdown and control  
461 cells were tested by western blotting with antibodies directed to CTS defense (Invitrogen, BMS1032),  
462 CCZ1 (Santa Cruz Biotechnology, sc-514290), EDC4 (Cell Signaling Technology, 2548S), and  
463 actin as a loading control (Sigma-Aldrich, MAB1501R). Once knockdown was confirmed, cells  
464 were infected with SARS-CoV-2 or OC43 at MOI 0.01 and RNA was extracted at 2 dpi for viral  
465 genome copy number enumeration, as described above.

466

467 **Identification and testing inhibitors of host factors from CRISPR screens**

468 Online databases and published literature were used to find small molecule inhibitors targeting a  
469 subset of top-scoring genes in the CRISPR screens. Amlexanox was purchased from InvivoGen.  
470 Abemaciclib, AZ1, carfilzomib, olaparib, and nintedanib were purchased from Selleckchem.  
471 Harmine, INDY, chlorpromazine, promethazine, UC2288, and CID 1067700 were purchased from  
472 Millipore Sigma. Drugs were diluted according to the manufacturers' recommendations and  
473 single-use aliquots were frozen at -80°C until the time of assay. Drugs were diluted down to 2X  
474 concentrations and mixed with 2X concentrations of virus to generate 1X concentrations, then  
475 added to the monolayers. Cells were infected at a MOI of 0.2 as determined by preliminary  
476 experiments to generate an ideal dynamic range of the colorimetric CytoTox 96 ® Non-  
477 Radioactive Cytotoxicity Assay (Promega). Infections progressed for 72 h at which time  
478 supernatant from treatments and controls were processed for LDH release according to the  
479 manufacturer's recommendations. Absorbance at 450 nm was read using an accuSkan FC  
480 microplate reader (Fisher Scientific) with SkanIt software (Fisher Scientific). Absorbance values  
481 were background subtracted and transformed to percent of virus-infected controls. These  
482 percentages were compared to the values obtained from virus infected-cell cytotoxicity values by  
483 one-way ANOVA using GraphPad Prism version 9. Assays were carried out in biological duplicate  
484 and in three independent experiments. The concentration of drug alone that resulted in 50% of  
485 maximum toxicity (inhibitory concentration 50; IC<sub>50</sub>) and the concentration of drug that inhibited  
486 50% of the vehicle treated SARS-CoV-2 induced cytotoxicity (effective concentration 50; EC<sub>50</sub>)  
487 were determined by serially diluting small molecule inhibitors during SARS-CoV-2 infection of  
488 Vero E6 cells. EC<sub>50</sub> and IC<sub>50</sub> values were calculated by transforming inhibitor concentrations to  
489 log then using the non-linear fit with variable slope function (GraphPad Prism version 9) to  
490 determine best fit variables using the percent of maximum SARS-CoV-2 induced cytotoxicity  
491 measurements at each drug concentration performed in technical duplicate.

492

493 **Website creation and data repository:**

494 To facilitate the access, reusability and integration of this data, we have created and hosted a  
495 website ([sarscrisprscreens.epi.ufl.edu](http://sarscrisprscreens.epi.ufl.edu)) which contains data for previously published HCoV  
496 CRISPR screens and our integrated MAGeCK analysis using the VISPR pipeline of the SARS-  
497 CoV-2 screens. Our goal is to provide a community resource for facile integrated analysis of  
498 current and future CRISPR screens. Further details on how to submit new data is provided on the  
499 website and in supplemental methods.

500

501 **Statistical analysis**

502 For the genome-scale CRISPR analysis, the embedded statistical tools in the MAGeCK/VISPR  
503 pipelines were used (15, 36). Further details are provided in the supplemental materials. All other  
504 statistical analyses were carried out using GraphPad Prism 9.0. To compare the mean normalized  
505 viral genome copy number values in targeted shRNA knockdown experiments (Fig. 6), *P* values  
506 were determined using one-way ANOVA test (\**P* < 0.05, \*\**P* < 0.01, \*\*\**P* < 0.001), with error  
507 bars representing standard errors of mean (*n* = 3 experiments). For testing inhibitory activity of  
508 small molecules on SARS-CoV-2 infection of Vero E6 cells (Fig. 7), a one-way ANOVA test was  
509 used for comparison of toxicity values for inhibitor-treated infected cells and infected-only control  
510 cells (no treatment), with error bars denoting standard deviation for all panels (*n* = 3 experiments).  
511 Non-linear regression of data points was used to determine the EC<sub>50</sub> and IC<sub>50</sub> values for indicated  
512 compounds.

513

514

515 **References**

516

- 517 1. E. Hartenian, D. Nandakumar, A. Lari, M. Ly, J. M. Tucker, B. A. Glaunsinger, The  
518 molecular virology of coronaviruses, *J Biol Chem* **295**, 12910–12934 (2020).
- 519 2. S. Ghosh, T. A. Dellibovi-Ragheb, A. Kerviel, E. Pak, Q. Qiu, M. Fisher, P. M. Takvorian, C.  
520 Bleck, V. W. Hsu, A. R. Fehr, S. Perlman, S. R. Achar, M. R. Straus, G. R. Whittaker, C. A. M.  
521 de Haan, J. Kehrl, G. Altan-Bonnet, N. Altan-Bonnet,  $\beta$ -Coronaviruses Use Lysosomes for  
522 Egress Instead of the Biosynthetic Secretory Pathway, *Cell* **183**, 1520-1535.e14 (2020).
- 523 3. Y. Wang, F. Jin, R. Wang, F. Li, Y. Wu, K. Kitazato, Y. Wang, HSP90: a promising broad-  
524 spectrum antiviral drug target, *Arch Virol* **162**, 3269–3282 (2017).
- 525 4. Y. Debing, J. Neyts, L. Delang, The future of antivirals: broad-spectrum inhibitors, *Curr Opin  
526 Infect Dis* **28**, 596–602 (2015).
- 527 5. Y. Zhu, F. Feng, G. Hu, Y. Wang, Y. Yu, Y. Zhu, W. Xu, X. Cai, Z. Sun, W. Han, R. Ye, D.  
528 Qu, Q. Ding, X. Huang, H. Chen, W. Xu, Y. Xie, Q. Cai, Z. Yuan, R. Zhang, A genome-wide  
529 CRISPR screen identifies host factors that regulate SARS-CoV-2 entry, *Nat Commun* **12**, 961  
530 (2021).
- 531 6. R. Wang, C. R. Simoneau, J. Kulsuptrakul, M. Bouhaddou, K. A. Travisano, J. M. Hayashi, J.  
532 Carlson-Steiner, J. R. Zengel, C. M. Richards, P. Fozouni, J. Oki, L. Rodriguez, B. Joehnk, K.  
533 Walcott, K. Holden, A. Sil, J. E. Carette, N. J. Krogan, M. Ott, A. S. Puschnik, Genetic Screens  
534 Identify Host Factors for SARS-CoV-2 and Common Cold Coronaviruses, *Cell* **184**, 106–119  
535 (2020).
- 536 7. W. M. Schneider, J. M. Luna, H.-H. Hoffmann, F. J. Sánchez-Rivera, A. A. Leal, A. W.  
537 Ashbrook, J. Le Pen, I. Ricardo-Lax, E. Michailidis, A. Peace, A. F. Stenzel, S. W. Lowe, M. R.  
538 MacDonald, C. M. Rice, J. T. Poirier, Genome-Scale Identification of SARS-CoV-2 and Pan-  
539 coronavirus Host Factor Networks, *Cell* **184**, 120-132.e14 (2021).

540 8. J. Wei, M. M. Alfajaro, P. C. DeWeirdt, R. E. Hanna, W. J. Lu-Culligan, W. L. Cai, M. S.  
541 Strine, S.-M. Zhang, V. R. Graziano, C. O. Schmitz, J. S. Chen, M. C. Mankowski, R. B. Filler,  
542 N. G. Ravindra, V. Gasque, F. J. de Miguel, A. Patil, H. Chen, K. Y. Oguntuyo, L. Abriola, Y.  
543 V. Surovtseva, R. C. Orchard, B. Lee, B. D. Lindenbach, K. Politi, D. van Dijk, C. Kadoch, M.  
544 D. Simon, Q. Yan, J. G. Doench, C. B. Wilen, Genome-wide CRISPR Screens Reveal Host  
545 Factors Critical for SARS-CoV-2 Infection, *Cell* **184**, 76–91 (2020).

546 9. Z. Daniloski, T. X. Jordan, H.-H. Wessels, D. A. Hoagland, S. Kasela, M. Legut, S. Maniatis,  
547 E. P. Mimitou, L. Lu, E. Geller, O. Danziger, B. R. Rosenberg, H. Phatnani, P. Smibert, T.  
548 Lappalainen, B. R. tenOever, N. E. Sanjana, Identification of Required Host Factors for SARS-  
549 CoV-2 Infection in Human Cells, *Cell* **184**, 92–105 (2020).

550 10. J. Baggen, L. Persoons, S. Jansen, E. Vanstreels, M. Jacquemyn, D. Jochmans, J. Neyts, K.  
551 Dallmeier, P. Maes, D. Daelemans, Identification of TMEM106B as proviral host factor for  
552 SARS-CoV-2, *Nat Genet* **53**, 435–444 (2021).

553 11. M. Hoffmann, H. Kleine-Weber, S. Schroeder, N. Krüger, T. Herrler, S. Erichsen, T. S.  
554 Schiergens, G. Herrler, N.-H. Wu, A. Nitsche, M. A. Müller, C. Drosten, S. Pöhlmann, SARS-  
555 CoV-2 Cell Entry Depends on ACE2 and TMPRSS2 and Is Blocked by a Clinically Proven  
556 Protease Inhibitor, *Cell* **181**, 271-280.e8 (2020).

557 12. X. Zhao, F. Guo, F. Liu, A. Cuconati, J. Chang, T. M. Block, J.-T. Guo, Interferon induction  
558 of IFITM proteins promotes infection by human coronavirus OC43, *Proc Natl Acad Sci U S A*  
559 **111**, 6756–6761 (2014).

560 13. G. Shi, A. D. Kenney, E. Kudryashova, A. Zani, L. Zhang, K. K. Lai, L. Hall-Stoodley, R. T.  
561 Robinson, D. S. Kudryashov, A. A. Compton, J. S. Yount, Opposing activities of IFITM proteins  
562 in SARS-CoV-2 infection, *EMBO J* **40**, e106501 (2021).

563 14. H. Winstone, M. J. Lista, A. C. Reid, C. Bouton, S. Pickering, R. P. Galao, C. Kerridge, K. J.  
564 Doores, C. Swanson, S. Neil, The polybasic cleavage site in the SARS-CoV-2 spike modulates  
565 viral sensitivity to Type I interferon and IFITM2, *J Virol* (2021), doi:10.1128/JVI.02422-20.

566 15. W. Li, J. Köster, H. Xu, C.-H. Chen, T. Xiao, J. S. Liu, M. Brown, X. S. Liu, Quality control,  
567 modeling, and visualization of CRISPR screens with MAGeCK-VISPR, *Genome Biology* **16**,  
568 281 (2015).

569 16. J. G. Doench, N. Fusi, M. Sullender, M. Hegde, E. W. Vaimberg, K. F. Donovan, I. Smith, Z.  
570 Tothova, C. Wilen, R. Orchard, H. W. Virgin, J. Listgarten, D. E. Root, Optimized sgRNA  
571 design to maximize activity and minimize off-target effects of CRISPR-Cas9, *Nature  
572 Biotechnology* **34**, 184–191 (2016).

573 17. X. Ou, Y. Liu, X. Lei, P. Li, D. Mi, L. Ren, L. Guo, R. Guo, T. Chen, J. Hu, Z. Xiang, Z.  
574 Mu, X. Chen, J. Chen, K. Hu, Q. Jin, J. Wang, Z. Qian, Characterization of spike glycoprotein of  
575 SARS-CoV-2 on virus entry and its immune cross-reactivity with SARS-CoV, *Nature  
576 Communications* **11**, 1620 (2020).

577 18. A. L. Bailey, M. S. Diamond, A Crisp(r) New Perspective on SARS-CoV-2 Biology, *Cell* **0**  
578 (2020), doi:10.1016/j.cell.2020.12.003.

579 19. J.-M. Heo, A. Ordureau, S. Swarup, J. A. Paulo, K. Shen, D. M. Sabatini, J. W. Harper,  
580 RAB7A phosphorylation by TBK1 promotes mitophagy via the PINK-PARKIN pathway, *Sci  
581 Adv* **4**, eaav0443 (2018).

582 20. O.-Y. Revach, S. Liu, R. W. Jenkins, Targeting TANK-binding kinase 1 (TBK1) in cancer,  
583 *null* **24**, 1065–1078 (2020).

584 21. M. Su, Y. Chen, S. Qi, D. Shi, L. Feng, D. Sun, A Mini-Review on Cell Cycle Regulation of  
585 Coronavirus Infection, *Front. Vet. Sci.* **7** (2020), doi:10.3389/fvets.2020.586826.

586 22. T. Thamamongood, A. Aebsicher, V. Wagner, M. W. Chang, R. Elling, C. Benner, A.  
587 García-Sastre, G. Kochs, M. Beer, M. Schwemmle, A Genome-Wide CRISPR-Cas9 Screen  
588 Reveals the Requirement of Host Cell Sulfation for Schmallenberg Virus Infection, *J Virol* **94**  
589 (2020), doi:10.1128/JVI.00752-20.

590 23. H. Gao, Y. Lin, J. He, S. Zhou, M. Liang, C. Huang, X. Li, C. Liu, P. Zhang, Role of heparan  
591 sulfate in the Zika virus entry, replication, and cell death, *Virology* **529**, 91–100 (2019).

592 24. R. J. Park, T. Wang, D. Koundakjian, J. F. Hultquist, P. Lamothe-Molina, B. Monel, K.  
593 Schumann, H. Yu, K. M. Krupczak, W. Garcia-Beltran, A. Piechocka-Trocha, N. J. Krogan, A.  
594 Marson, D. M. Sabatini, E. S. Lander, N. Hacohen, B. D. Walker, A genome-wide CRISPR  
595 screen identifies a restricted set of HIV host dependency factors, *Nature Genetics* **49**, 193–203  
596 (2017).

597 25. S. Minamisawa, M. Hoshijima, G. Chu, C. A. Ward, K. Frank, Y. Gu, M. E. Martone, Y.  
598 Wang, J. Ross Jr, E. G. Kranias, Chronic phospholamban–sarcoplasmic reticulum calcium  
599 ATPase interaction is the critical calcium cycling defect in dilated cardiomyopathy, *Cell* **99**,  
600 313–322 (1999).

601 26. T. Kushibiki, T. Nakamura, M. Tsuda, T. Tsuchikawa, K. Hontani, K. Inoko, M. Takahashi,  
602 T. Asano, K. Okamura, S. Murakami, Role of dimerized C16orf74 in aggressive pancreatic  
603 cancer: a novel therapeutic target, *Molecular cancer therapeutics* **19**, 187–198 (2020).

604 27. T. Nakamura, T. Katagiri, S. Sato, T. Kushibiki, K. Hontani, T. Tsuchikawa, S. Hirano, Y.  
605 Nakamura, Overexpression of C16orf74 is involved in aggressive pancreatic cancers, *Oncotarget*  
606 **8**, 50460 (2017).

607 28. P. Dhillon, C. D. Rao, Rotavirus Induces Formation of Remodeled Stress Granules and P  
608 Bodies and Their Sequestration in Viroplasms To Promote Progeny Virus Production, *J Virol* **92**  
609 (2018), doi:10.1128/JVI.01363-18.

610 29. C. J. Beckham, R. Parker, P Bodies, Stress Granules, and Viral Life Cycles, *Cell Host &  
611 Microbe* **3**, 206–212 (2008).

612 30. C.-A. Robinson, M. Kleer, R. P. Mulloy, E. L. Castle, B. Q. Boudreau, J. A. Corcoran,  
613 Human coronaviruses disassemble processing bodies, *bioRxiv*, 2020.11.08.372995 (2020).

614 31. C. Z. Chen, M. Xu, M. Pradhan, K. Gorshkov, J. D. Petersen, M. R. Straus, W. Zhu, P.  
615 Shinn, H. Guo, M. Shen, C. Klumpp-Thomas, S. G. Michael, J. Zimmerberg, W. Zheng, G. R.  
616 Whittaker, Identifying SARS-CoV-2 Entry Inhibitors through Drug Repurposing Screens of  
617 SARS-S and MERS-S Pseudotyped Particles, *ACS Pharmacol Transl Sci* (2020),  
618 doi:10.1021/acsptsci.0c00112.

619 32. L. R. Reznikov, M. H. Norris, R. Vashisht, A. P. Bluhm, D. Li, Y.-S. J. Liao, A. Brown, A. J.  
620 Butte, D. A. Ostrov, Identification of antiviral antihistamines for COVID-19 repurposing,  
621 *Biochem Biophys Res Commun* **538**, 173–179 (2021).

622 33. L. L. Hammitt, S. Kazungu, S. Welch, A. Bett, C. O. Onyango, R. N. Gunson, J. A. G. Scott,  
623 D. J. Nokes, Added value of an oropharyngeal swab in detection of viruses in children  
624 hospitalized with lower respiratory tract infection, *J Clin Microbiol* **49**, 2318–2320 (2011).

625 34. S. M. Nabokina, K. Inoue, V. S. Subramanian, J. E. Valle, H. Yuasa, H. M. Said, Molecular  
626 Identification and Functional Characterization of the Human Colonic Thiamine Pyrophosphate  
627 Transporter, *J Biol Chem* **289**, 4405–4416 (2014).

628 35. O. Shalem, N. E. Sanjana, E. Hartenian, X. Shi, D. A. Scott, T. S. Mikkelsen, D. Heckl, B. L.  
629 Ebert, D. E. Root, J. G. Doench, F. Zhang, Genome-Scale CRISPR-Cas9 Knockout Screening in  
630 Human Cells, *Science* **343**, 84 (2014).

631 36. W. Li, H. Xu, T. Xiao, L. Cong, M. I. Love, F. Zhang, R. A. Irizarry, J. S. Liu, M. Brown, X.  
632 S. Liu, MAGeCK enables robust identification of essential genes from genome-scale  
633 CRISPR/Cas9 knockout screens, *Genome Biology* **15**, 554 (2014).

634 37. W. C. Warren, A. J. Jasinska, R. García-Pérez, H. Svärdal, C. Tomlinson, M. Rocchi, N.  
635 Archidiacono, O. Capozzi, P. Minx, M. J. Montague, K. Kyung, L. W. Hillier, M. Kremitzki, T.  
636 Graves, C. Chiang, J. Hughes, N. Tran, Y. Huang, V. Ramensky, O.-W. Choi, Y. J. Jung, C. A.  
637 Schmitt, N. Juretic, J. Wasserscheid, T. R. Turner, R. W. Wiseman, J. J. Tuscher, J. A. Karl, J. E.  
638 Schmitz, R. Zahn, D. H. O'Connor, E. Redmond, A. Nisbett, B. Jacquelin, M. C. Müller-  
639 Trutwin, J. M. Brenchley, M. Dione, M. Antonio, G. P. Schroth, J. R. Kaplan, M. J. Jorgensen,  
640 G. W. C. Thomas, M. W. Hahn, B. J. Raney, B. Aken, R. Nag, J. Schmitz, G. Churakov, A. Noll,  
641 R. Stanyon, D. Webb, F. Thibaud-Nissen, M. Nordborg, T. Marques-Bonet, K. Dewar, G. M.  
642 Weinstock, R. K. Wilson, N. B. Freimer, The genome of the vervet (*Chlorocebus aethiops*  
643 *sabaeus*), *Genome Res* **25**, 1921–1933 (2015).

644 38. A. McKenna, J. Shendure, FlashFry: a fast and flexible tool for large-scale CRISPR target  
645 design, *BMC Biol* **16**, 74 (2018).

646 39. M. Schaefer, D.-A. Clevert, B. Weiss, A. Steffen, PAVOOC: designing CRISPR sgRNAs  
647 using 3D protein structures and functional domain annotations, *Bioinformatics* **35**, 2309–2310  
648 (2019).

649 40. W. Li, H. Xu, T. Xiao, L. Cong, M. I. Love, F. Zhang, R. A. Irizarry, J. S. Liu, M. Brown, X.  
650 S. Liu, MAGeCK enables robust identification of essential genes from genome-scale  
651 CRISPR/Cas9 knockout screens, *Genome Biol* **15**, 554 (2014).

652 41. M. Wegner, K. Husnjak, M. Kaulich, Unbiased and Tailored CRISPR/Cas gRNA Libraries  
653 by Synthesizing Covalently-closed-circular (3Cs) DNA, *Bio-protocol* **10**, e3472 (2020).

654 42. J. Joung, S. Konermann, J. S. Gootenberg, O. O. Abudayyeh, R. J. Platt, M. D. Brigham, N.  
655 E. Sanjana, F. Zhang, Genome-scale CRISPR-Cas9 knockout and transcriptional activation  
656 screening, *Nat Protoc* **12**, 828–863 (2017).

657 43. The COVID-19 Drug and Gene Set Library (available at <https://maayanlab.cloud/covid19>).

658

659 **Acknowledgments:** We thank Dr. John Lednicky (University of Florida, UF) and the UF Health  
660 Cancer Center for providing key reagents. This work was supported by the UF Clinical and  
661 Translational Science Institute. S.M.K. and M.G. were further supported by NIH R01AI123144.

662 **Author contributions:**

663 Conceptualization: MHN, SMK, CDV  
664 Methodology: MG, APB, MS, AT, MHN, SMK, CDV  
665 Investigation: MG, APB, MS, AT, MR, AS, RR, MHN  
666 Funding acquisition: MHN, SMK, CDV  
667 Project administration: MHN, SMK, CDV  
668 Supervision: MHN, SMK, CDV  
669 Writing – original draft: MG, APB  
670 Writing – review & editing: MHN, SMK, CDV

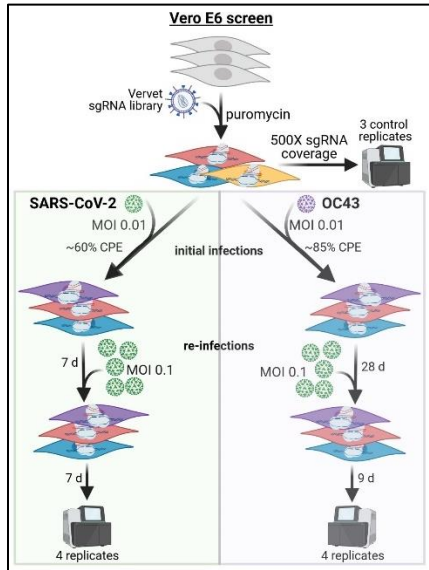
671 **Competing interests:** A patent entitled Methods of Treatment for SARS-CoV-2 Infections  
672 (PROV Appl. No. 63/145,763) was filed on February 4, 2021.

673 **Data and materials availability:** All data are available in the main text or the supplementary  
674 materials.

675

676 **Figures**

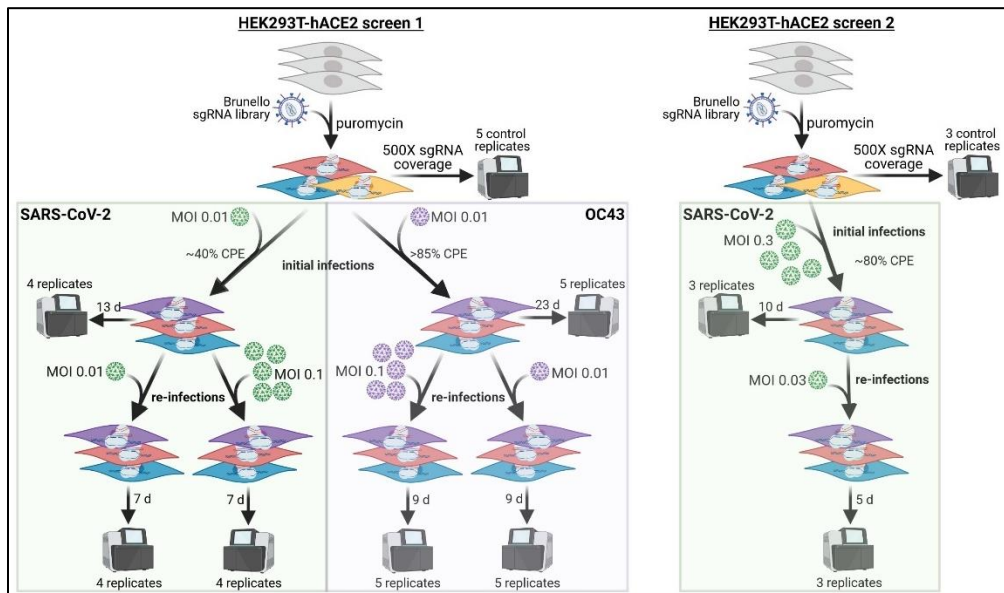
677 **A**



678

679

680 **B**



681

682

683

684

685

686

687

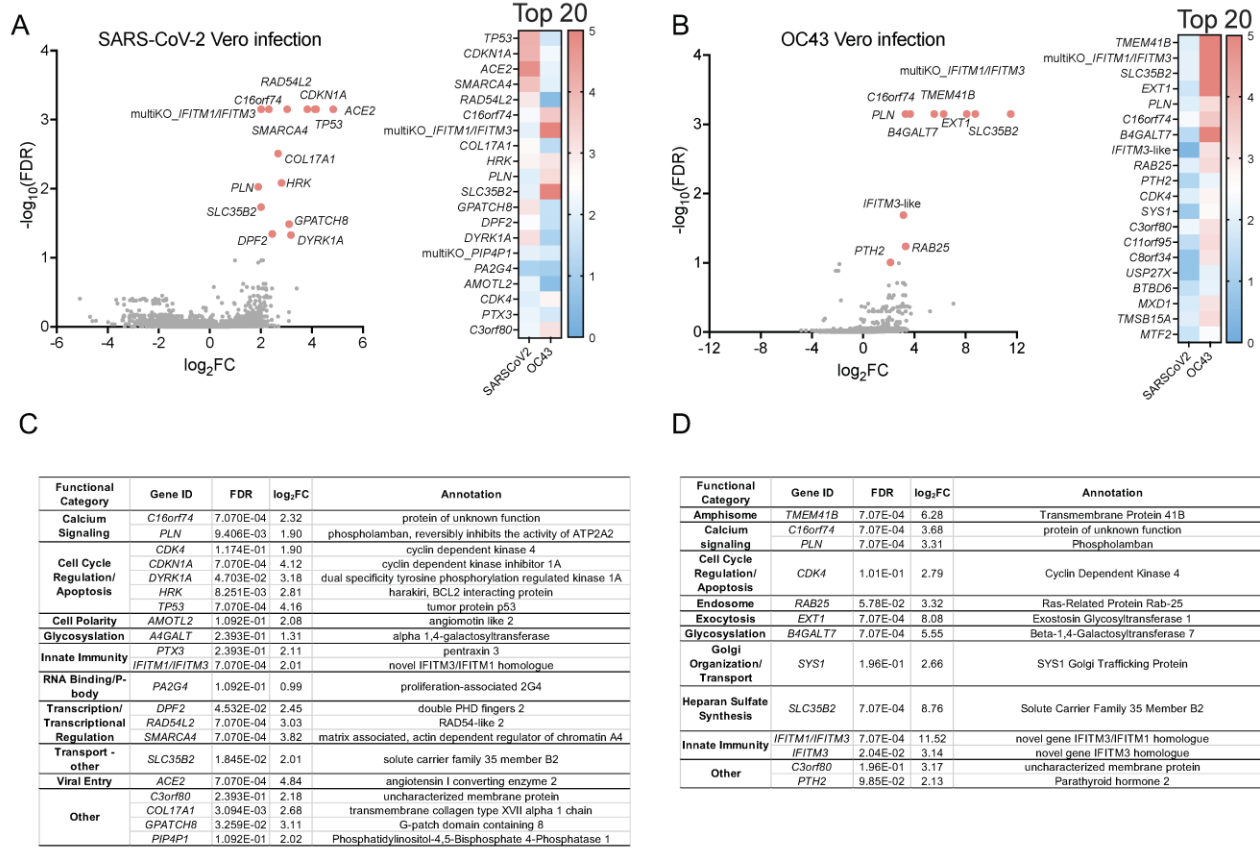
688

689

690

691

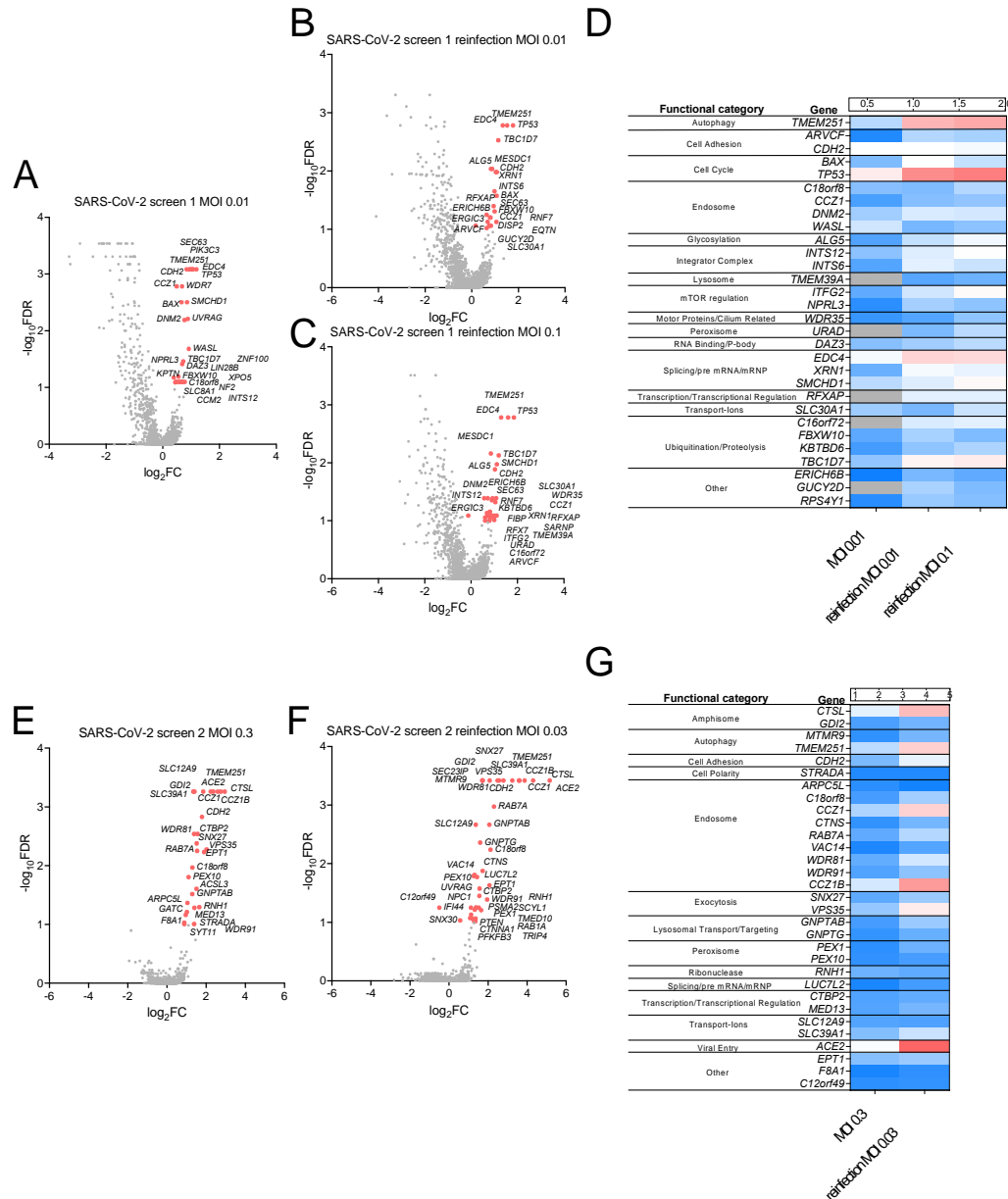
**Figure 1. Experimental design for genome-scale CRISPR screens performed in this study.** Details of these screens are provided in the methods. **A)** Vero E6 cells transduced with the newly generated Vervet sgRNA library were infected with SARS-CoV-2 or OC43 at MOI 0.01, resistant cells were expanded and re-infected at MOI 0.1. **B)** Two screens were performed in HEK293T-hACE2 cells transduced with the Brunello sgRNA library. In the first screen, cells were infected with SARS-CoV-2 or OC43 at MOI 0.01 and resistant cells were re-infected with either MOI 0.01 or MOI 0.1 of the corresponding virus. In the second screen, cells with infected with SARS-CoV-2 at MOI 0.3 and re-infected at MOI 0.03. In all cases, genomic DNA was extracted from multiple replicates of control cells, the initial infections, and re-infections for the purpose of sgRNA sequencing.



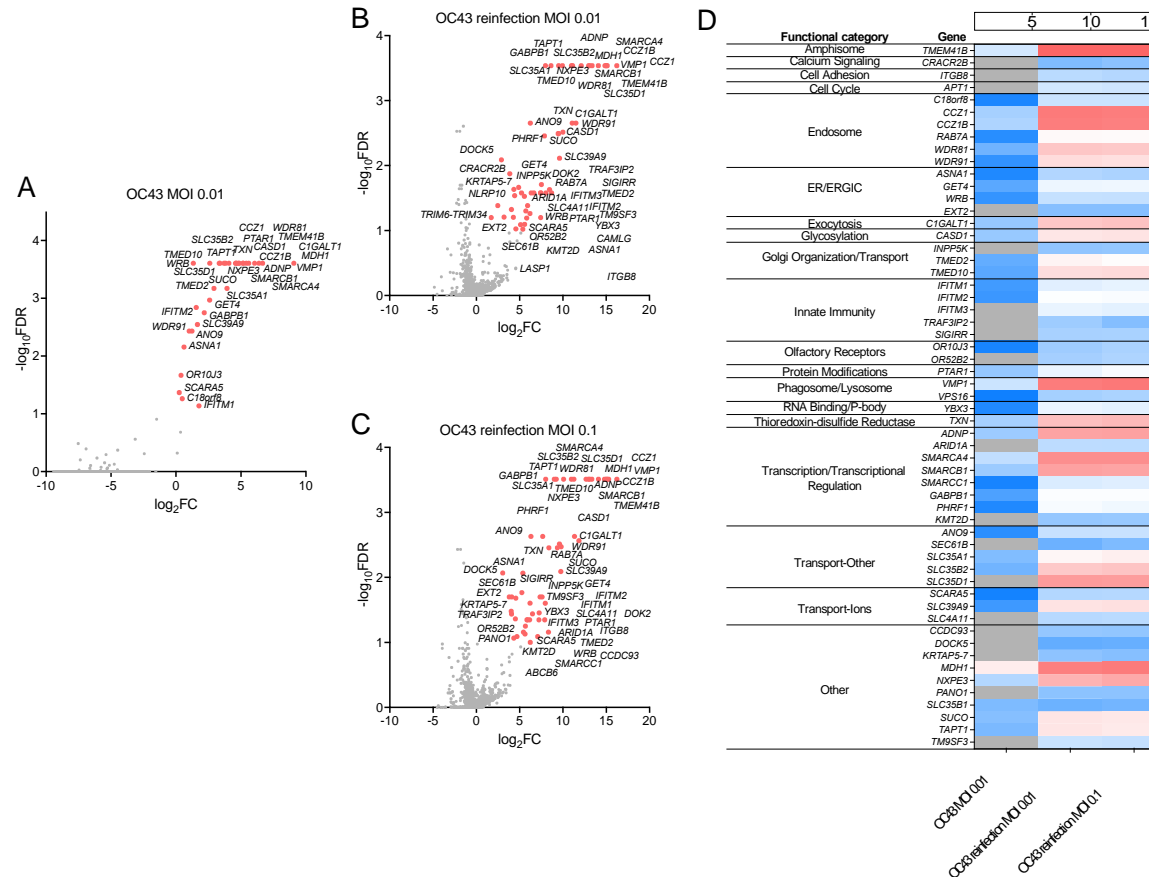
692  
693

**Fig 2. Identification of host factors that promote HCoV infection of Vero E6 cells.** Vero E6 cells transduced with a *C. sabaeus*-specific sgRNA library were infected with SARS-CoV-2 or OC43 at MOI 0.01, resistant cells reinfected at MOI 0.01, and sgRNAs in resistant clones sequenced. MAGeCK analysis of multiple replicates compared to uninfected control library replicates yielded  $\log_2$ fold changes ( $\log_2 FC$ ) that were plotted on the x-axis. Negative  $\log_{10}$  transformed false discovery rates (FDR) were plotted on the y-axis. Data are presented for SARS-CoV-2 (**A**) and OC43 (**B**) Vero E6 infections. The heat maps display the  $\log_2 FC$  for the 20 top-scoring genes comparing results for SARS-CoV-2 and OC43 infections. Genes targeted by significantly enriched sgRNAs ( $FDR < 0.25$ ) were segregated into functional categories using PANTHER for SARS-CoV-2 (**C**) and OC43 (**D**) infections.

704



705  
706 **Fig 3. Identification of host factors that promote SARS-CoV-2 infection of HEK293T-hACE2**  
707 cells. HEK293T-hACE2 cells transduced with the Brunello sgRNA library were infected with  
708 SARS-CoV-2 at MOI 0.01 and sgRNAs in resistant clones sequenced. Resistant clones were  
709 reinjected with SARS-CoV-2 at MOI 0.01 or MOI 0.1 and sgRNAs in resistant clones sequenced.  
710 For all three infections, MAGeCK analysis of multiple replicates compared to uninfected control  
711 library replicates yielded log<sub>2</sub>fold changes (log<sub>2</sub>FC) that were plotted on the x-axis. Negative log<sub>10</sub>  
712 transformed FDR were plotted on the y-axis. Data are presented for the initial infection (A), MOI  
713 0.01 reinfection (B), and MOI 0.1 reinfection (C). D) The heatmap displays the log<sub>2</sub>FC for top-  
714 scoring genes (FDR<0.1) across the three infections. The entire experiment was repeated at MOI  
715 0.3, with sgRNAs sequenced from resistant clones in the initial infection (E) and reinfection (F).  
716 G) The heatmap displays the log<sub>2</sub>FC for top-scoring genes (FDR<0.25) across the two infections.  
717

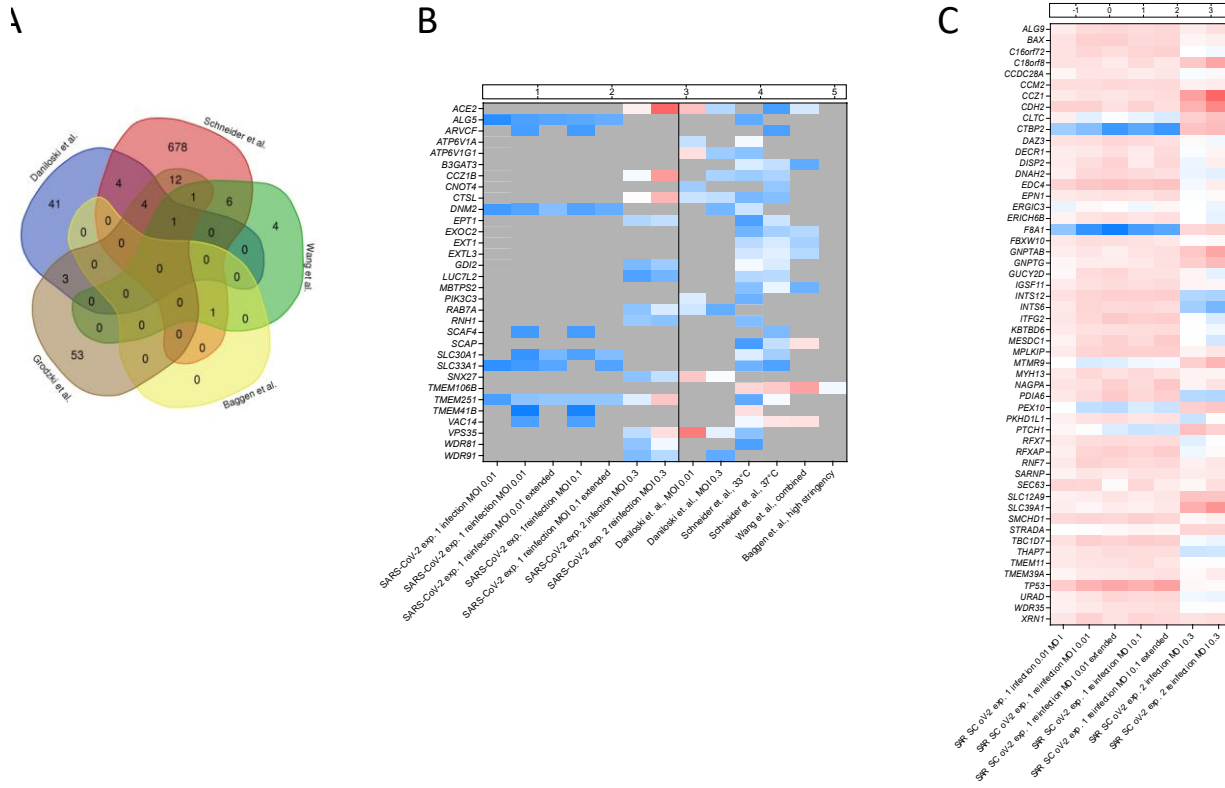


718

**Fig 4. Identification of host factors that promote OC43 infection of HEK293T-hACE2 cells.**  
 HEK293T-hACE2 cells transduced with the Brunello sgRNA library were infected with OC43 at MOI 0.01 and sgRNAs in resistant clones sequenced. Resistant clones were reinfected with OC43 at MOI 0.01 or MOI 0.1 and sgRNAs in resistant clones sequenced. For all three infections, MAGeCK analysis of multiple replicates compared to uninfected control library replicates yielded log<sub>2</sub> fold changes (log<sub>2</sub>FC) that were plotted on the x-axis. Negative log<sub>10</sub> transformed FDR were plotted on the y-axis. Data are presented for the initial infection (A), MOI 0.01 reinfection (B), and MOI 0.1 reinfection (C). D) The heat map displays the log<sub>2</sub>FC for top-scoring genes (FDR<0.25) across the three infections.

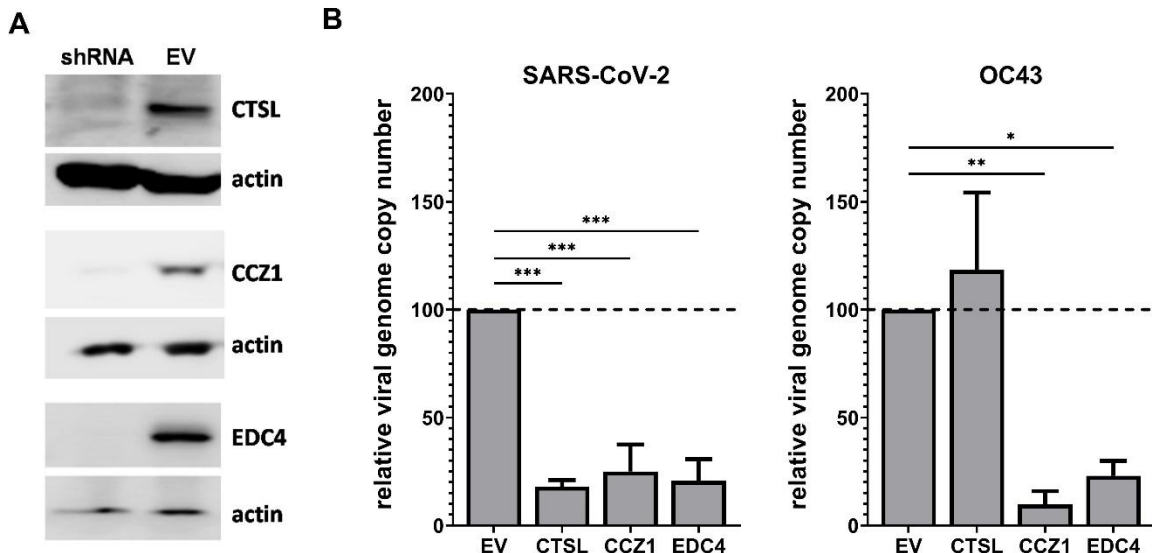
727

728

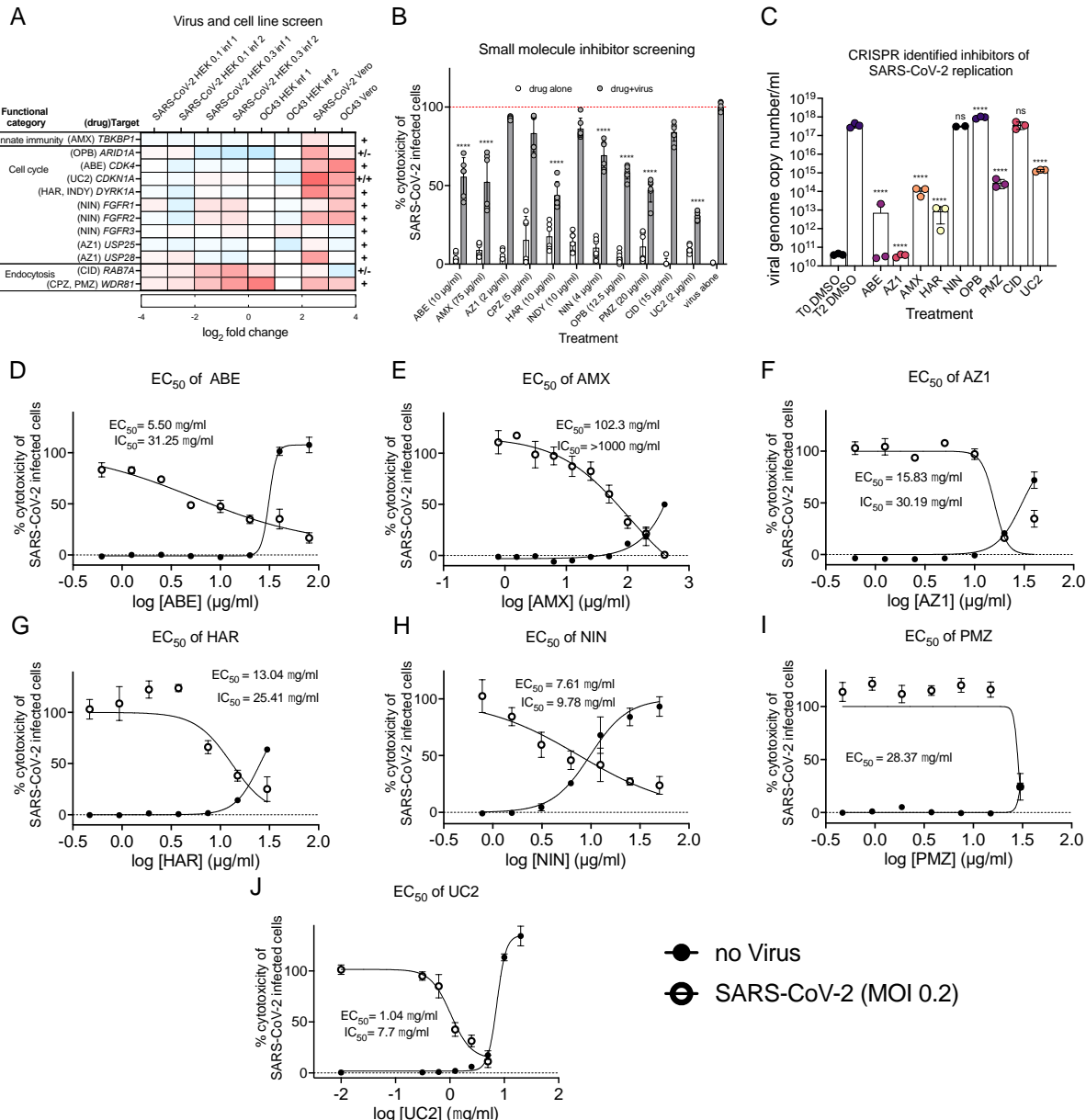


729  
730 **Fig 5. Comparison of multiple CRISPR screens identifying host factors promoting SARS-**  
731 **CoV-2 infection of human cell lines.** A) Data from four recently published CRISPR screens for  
732 SARS-CoV-2 in various human cell lines were reanalyzed and compared to our data to identify  
733 common top-scoring genes (FDR<0.25). Using this criterion, there were 74 genes identified in our  
734 study, 53 in Daniloski et al., 707 in Schneider et al., 13 in Wang et al., and 1 in Baggen et al. No  
735 common genes were identified in all studies, 1 gene was identified in four studies, 6 genes were  
736 identified in three studies, and 25 genes were identified in two studies. 53 genes were uniquely  
737 identified in our study as significant. B) The heat map displays the log<sub>2</sub>FC for the 32 genes found  
738 in common across two or more of the published studies with FDR<0.25. C) A heat map displaying  
739 the log<sub>2</sub>FC for the 53 genes uniquely identified as significant in our studies compared to their  
740 observed log<sub>2</sub>FC across the other published studies.

741



742  
743 **Fig 6. Confirmation of host factor involvement by targeted shRNA knockdown.** Lentivirus-  
744 packaged shRNA clones directed to *CTSL*, *CCZ1*, and *EDC4* were transduced into HEK293T-  
745 hACE2 cells and selected with puromycin. **A**) Gene knockdown was assessed using western  
746 blotting with antibodies directed to *CTSL*, *CCZ1*, and *EDC4* in cells transduced with a gene-  
747 specific shRNA or empty vector control (EV). Actin expression served as a loading control. **B**)  
748 Triplicate wells of knockdown cells were infected with SARS-CoV-2 or OC43 at MOI 0.01. At 2  
749 dpi, viral genome copy numbers were determined by RT-qPCR and normalized to *GAPDH* levels  
750 as a housekeeping control. The data are reported as the relative normalized viral genome copy  
751 number in shRNA-expressing cells compared to the EV control ( $n = 3$  experiments). Error bars  
752 denote standard errors of mean and  $P$  values were determined using one-way ANOVA (\* $P < 0.05$ ,  
753 \*\* $P < 0.01$ , \*\*\* $P < 0.001$ ).

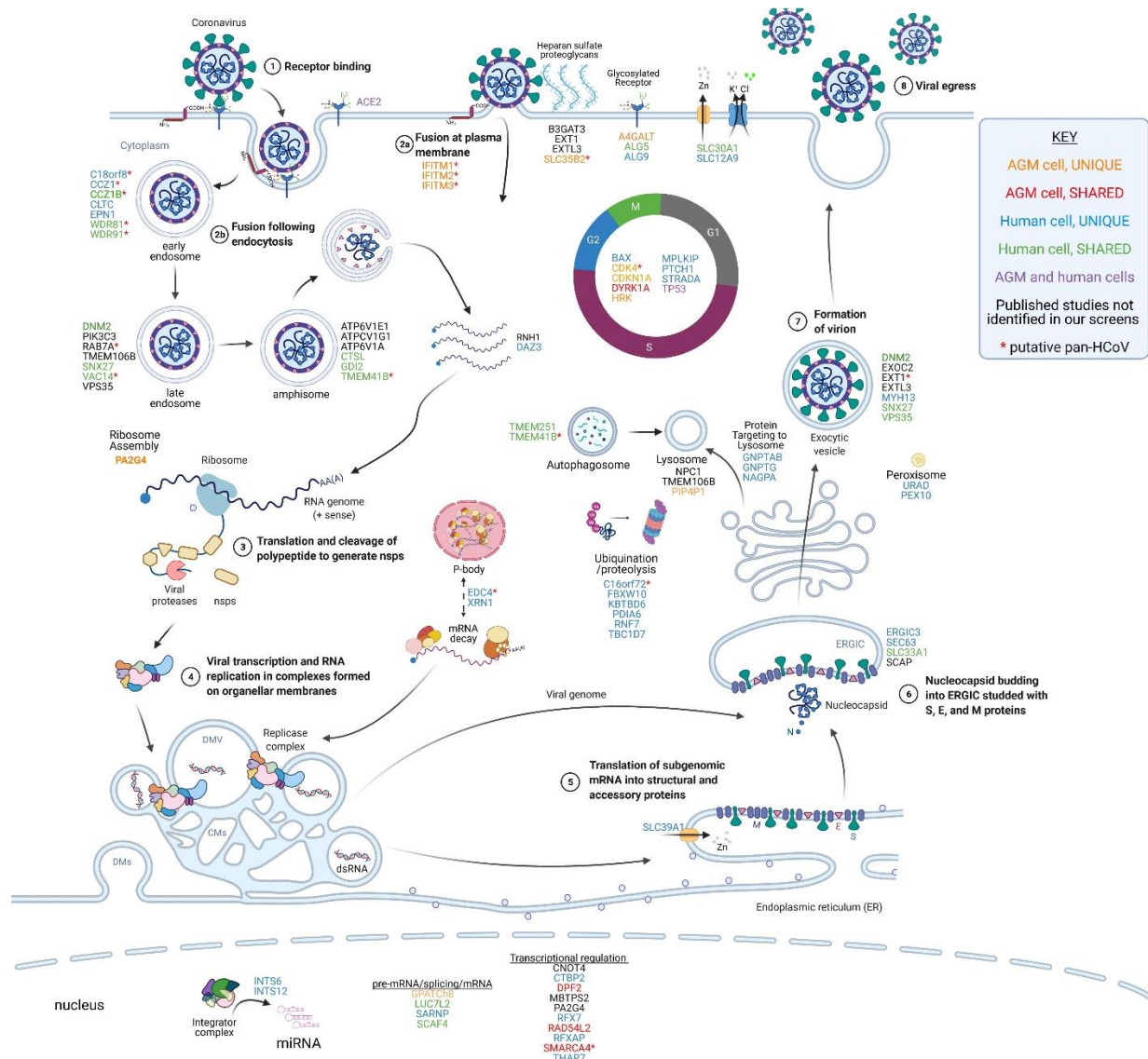


754

755

756

**Fig 7. Small molecules to CRISPR-identified targets inhibit SARS-CoV-2 infection. A)** The log<sub>2</sub>FC across the studies performed in this work for the 12 gene targets that had commercially available inhibitors. The + and - signs to the right of the heat map summarize the ability of these small molecules to prevent SARS-CoV-2 infection of Vero E6 cells. **B)** Initial screening of drug inhibition of SARS-CoV-2-induced cytotoxicity in Vero E6 cells following MOI 0.3 infection. **C)** Drug inhibition of SARS-CoV-2 genome replication was measured by RT-qPCR at 2 dpi of Vero E6 cells at MOI 0.01. One-way ANOVA was used to compare inhibitor-treated toxicity values to virus-alone controls. **D-J)** The EC<sub>50</sub> (ability of inhibitors to reduce SARS-CoV-2 cytotoxicity) and IC<sub>50</sub> (toxicity of inhibitors alone) curves were obtained by cytotoxicity assays in Vero E6 cells. Non-linear regression of the data points was used to determine the EC<sub>50</sub> and IC<sub>50</sub> values. Error bars indicate standard deviation for all panels (n = 3).



768

769

770

771

772

773

774

775

776

777

778

779

780

781

782

783

**Fig. 8. Summary of genes found in this and other studies and their potential roles in the SARS-CoV-2 life cycle.** The host factors identified in CRISPR screens are presented adjacent to the putative stage of viral replication where they function. The genes are color-coded based on their identification in our and other published studies, as indicated in the legend. Candidate pan-HCoV host factors are indicated with red asterisks. The virus replicates through a series of well-defined molecular steps. **1-2)** After virion binding to ACE2, SARS-CoV-2 can fuse at the plasma membrane or following endocytosis. Heparan sulfate proteoglycans enhance viral attachment to cells so host factors involved in heparan sulfate biosynthesis (B3GAT3, EXT1, EXT13, SLC35B2) and glycosylation (A4GALT, ALG5, ALG9) may play a role in viral entry. The IFITM proteins are proposed to promote fusion at the cell surface but inhibit fusion in endosomes. Host factors involved in endocytosis (C18orf8, CCZ1, CCZ1B, CLTC, EPN1, WDR81, WDR91), vesicular transport (DNM2, PIK3C3, RAB7A, TMEM106B, SNX27, VAC14, VPS35), and amphisome maturation/lysosome fusion (ATP6V1E1, ATPCV1G1, ATP6V1A, CTS, GDI2, TMEM41B) likely facilitate virion uncoating. **3)** The positive-sense RNA genome is then translated to produce the nonstructural polyproteins which are co-translationally cleaved to form

784 the mature nsps. Certain host factors like RNH1 and DAZ3 may serve to protect the viral genome  
785 from degradation by host enzymes. **4)** The nsps form the viral replicase which assembles on  
786 organellar membranes to form the replication and transcription complexes (RTCs) where progeny  
787 genomes and structural/accessory protein transcripts are produced, respectively. P-body  
788 components EDC4 and XRN1, identified in this study, may play a role in the maintaining viral  
789 RNA stability or assembly of the RTC. **5)** Structural and accessory proteins are translated, and  
790 structural proteins insert into the ER membrane. ER-localized SLC39A1 may play a role in this  
791 process. **6)** Nucleocapsids bud into the ERGIC, potentially aided by host factors ERGIC3, SEC63,  
792 SLC33A1, and SCAP. **7)** Progeny virions form as they traverse through the Golgi and structural  
793 proteins are glycosylated. **8)** Virions exit the cell through either typical exocytosis (DNM2,  
794 EXOC2, EXT1, EXTL3, MYH13, SNX27, VPS35) or nonclassical lysosomal egress (GNPTAB,  
795 GNPTG, NAGPA, NPC1, TMEM106B, PIP4P1). Numerous host factors with less obvious direct  
796 roles in promoting steps in the viral life cycle have also been identified in CRISPR screens. For  
797 example, numerous factors regulating the cell cycle (BAX, CDK4, CDKN1A, DYRK1A, HRK,  
798 MPLKIP, PTCH1, STRADA, TP53) were identified in our screens in AGM and human cells.  
799 Furthermore, multiple nuclear-localized host factors including diverse transcriptional regulators  
800 and two components of the integrator complex (INTS6, INTS12) were identified. Overall, the large  
801 number of diverse host factors that promote SARS-CoV-2 replication illustrates the large-scale  
802 exploitation of cellular processes required for successful viral propagation. Adapted from  
803 BioRender template titled Life Cycle of Coronavirus generated by the Britt Glaunsinger  
804 laboratory. Created with BioRender.com.